Mechanical Properties And Joining Mechanism of Magnetic Pulse Welded Aluminum To Titanium

Shujun Chen
Beijing University of Technology
Yang Han
Beijing University of Technology
Wentao Gong
Chinese Academy of Sciences Aerospace Information Research Institute
Tao Yuan (ty29@bjut.edu.cn)
Beijing University of Technology
Xiaoqing Jiang
Beijing University of Technology

Research Article

Keywords: Magnetic pulse welding, process parameters, impacting mode, joining mechanism

Posted Date: November 1st, 2021

DOI: https://doi.org/10.21203/rs.3.rs-1014220/v1

Abstract

Magnetic pulse welding of dissimilar aluminum and titanium was investigated to optimize process parameters in terms of discharge voltage, radial gap and overlapping length. Moreover, impacting modes at different overlapping lengths were discussed. The joining mechanism was analyzed from aspects of microstructure, composition and hardness distribution. The shear strength increased with increasing discharge voltages, whereas shear strength decreased at first and then increased with the increasing radial gap, which has a more significant influence on shear strength than discharge voltage. Three impacting modes were proposed as bidirectional impacting, overall impacting and single-orientation impacting. However, the single-orientation impacting mode has the highest effective joining ratio. The welded joints were divided into four transition layer interfaces: continuous transition zone, transition zone with cracks, intermittent transition zone, and non-transition zone. Waves and intermetallic compounds are the two characteristics of the Al-Ti joint welded by magnetic pulse welding. The metal's hardness near the joint surface is higher than that of the base metal. In addition, Al_3Ti and aluminum base metal were found in the transition layer of the joint.

1 Introduction

The lightweight components of aluminum alloys have been widely used in industrial fields for energy conservation and environmental protection, owing to their excellent overall properties [1–2]. Al-Ti components were fabricated for key load-bearing features in manufacturing fields such as aerospace and automobile [3]. However, metallurgical defects such as cracks easily occurred in the conventional fusion welding process due to significant properties differences between Ti and Al, resulting in a reduction of shear strength. Magnetic pulse welding (MPW), as a solid-state welding technology with high speed and environmental protection, can effectively eliminate the metallurgical defects in dissimilar Al-Ti with highly different physical properties.

MPW of aluminum and steel has been extensively studied, providing valuable information for MPWed Al and Ti. The process window for MPW of 1 mm thick Al to 0.25 mm thick stainless steel plates was investigated by Kore et al. [4] who found that tensile shear strength increased with increasing discharge voltage and the optimum standoff distance is 1.75 mm. Similarly, Lu et al. [5] explored the influence of process parameters on MPW of 1060 aluminum tube and AISI stainless steel rod. And they proposed that an invalid joining zone was prevented by reducing the overlapping length to 6 mm and shear strength increased with increasing discharge voltage but decreased with increasing radial gap. Manogaran et al. [6] observed two essential characteristics on the joint surface of AA1199 aluminum and EN355 steel plates welded by MPW. One is that the distribution of wave interface has a direction opposite to the weld center. The other is that intermetallic compounds (IMCs) are mainly composed of Fe_2Al_5 and $FeAl_3$. Furthermore, Yu et al. [7, 8] reported that element diffusion and grain refinement occurred near the joint interface of the Al-steel tube. Geng et al. [9, 10] also observed IMCs in MPW joint of 5 series Al and high strength steel and grain refinement due to the local melting of the interface by a high-speed impact process.

With the urgent demand for application of Al-Ti joining in recent years, especially in the aviation and aerospace field, MPW of Al-Ti plates has been studied. Nie et al. [11] studied MPW of TC4 plate and 3A21Al plate, and they found that surface roughness of the TC4 plate has a significant influence on ripple shape of the weld surface and wavelength increased with increasing surface roughness of TC4 plate. The results of the MPWed 3003Al and TC4 plate joint studied by Cui et al. [12] show that mechanical properties enhanced with increasing effective welding area and average thickness of the transition layer. However, as a highly efficient solid-phase technology, MPW has been widely used to join dissimilar materials with a special shape such as small tubular parts [13, 14]. However, research on MPW of Al and Ti tubular parts is still less. Mary et al. [15] studied the effect of radial gap on the morphology of the MPWed Al-Ti tube joint, and they reported that interlocking was formed between Al and Ti.

Moreover, a small gap leads to unbounded or limited joining. Both the impact speed and interface heating have enhanced with increasing radial gap and a large gap leads to cracks. To sum up, there are few studies on the other process parameters, such as process specifications and impacting mode. Besides, further investigation of the joining mechanism for MPWed Al-Ti is needed.

Therefore, considering the urgent needs of Al-Ti tube joining and existing research deficiencies, the present study aims to optimize process parameters for MPW of Al-Ti alloy, explore typical impact mode of the outer tube, and reveal joining mechanism for MPW of dissimilar Al-Ti tube.

2 Experimental Procedures

The base materials are 1060 Al tube (1 mm wall thickness) with a dimension of φ16 mm × 40 mm and TA1 Ti rod with a length of 45 mm and the diameter of the Ti rod is defined by the radial gap. The material properties of 1060 Al and TA1 Ti are shown in Table 1. The welding equipment is Pulsar 20-9 machine with a discharge frequency of 11.4 kHz. The welding process parameters are discharge voltage (U), radial gap (t), and overlapping length (l) between the outer tube and collector, as shown in Fig. 1, the free end is adjacent to the edge of the outer tube and the non-free end is close to the clamping end of the outer tube. Moreover, the rolling direction is parallel to the welding direction. The scope of the process window and experimental scheme was determined in Table 2 based on the previous experimental results.

Table 1
Physical properties of 1060Al and TA1 Ti materials

Material	Density/ kg•m-3	Electrical Resistivity/ Ω•m	Elastic Modulus/GPa	Tensile strength/MPa
1060 Al	2710	2.8×10-8	71	98
TA1 Ti	4500	4.2×10-8	107	430

Table 2
Welding process parameters for magnetic pulse welding of Al flyer and Ti rod

No.	Discharge voltage/kV	Radial gap/mm	overlapping length/mm
1#-5#	4.5	1, 1.25, 1.5, 1.75, 2	10
6#-10#	5	1, 1.25, 1.5, 1.75, 2	10
11#-15#	5.5	1, 1.25, 1.5, 1.75, 2	10
16#-20#	6	1, 1.25, 1.5, 1.75, 2	10
21#-25#	6.5	1, 1.25, 1.5, 1.75, 2	10
26#-30#	7	1, 1.25, 1.5, 1.75, 2	10
31#	6.5	2	4
32#	6.5	2	5
33#	6.5	2	6
34#	6.5	2	7
35#	6.5	2	8
36#	6.5	2	9
37#	6.5	2	10

Peeling tests and shear tests were carried out to explore the effect of microstructure on mechanical properties. Firstly, joints were sectioned into 1 mm thick pieces along the radial direction for the peeling experiment with two ends being clamped by calipers to peel off (Fig. 2(a)). Then, joining quality was judged by the macro morphology of the inner rod surface. Set the line corresponding to the guide groove of field shaper as 0 ° and take samples from 90 ° and 270 ° clockwise for peeling test. Fig. 2(b) shows a schematic drawing of the shear test. A 1mm thick circular slice was sectioned along the axial direction as the shear sample, the number of which was determined by overlapping length of the outer tube and inner rod. And the shear test was carried out by an electronic universal testing machine (CSS-1110) at a loading speed of 1 mm/min. The joint with a maximum shear strength above 30MPa is deemed as an effective joining. Moreover, the effective welding length L_C to overlapping length Lt ratio is defined as the effective joining ratio η. Moreover, hardness was tested by the SCTMC DHV-1000Z hardness tester. Finally, metallographic samples were sectioned along the cross-section and microstructure was analyzed by optical microscope (Olympus LEXT OLS4100 laser) and scanning electron microscope (FEI Quanta200) after grinding and polishing and the IMCs were detected by EDS (EDAX Genesis).

3 Results And Discussions

3.1 The Influence of process parameters on joint quality

3.1.1 Effect of discharge voltage on joint quality

Figure 3 shows shear strength and peel morphology of the joints at different discharge voltages, where the distribution of shear strength from left to right is a U-shaped curve and the joints are divided into three regions: zone I (left), zone II (center) and zone III (right), as shown in Figure 3(a), shear strength of the center region (zone II) is less than 30MPa with little residual metal in the inner rod after peeling, which is the invalid joining area. The shear strength of zone I and III is higher than that of zone II, with much more residual metal on the surface of the inner rod after peeling, indicating an effective joint zone. The strength of the magnetic field in the overlapping area decreased from the central field shaper to both sides, which was symmetrically distributed [16]. Resulting in the highest impact speed owing to the strongest magnetic field force that has been generated in the central field shaper and impact speed decreased along the axial direction to both sides. Due to the two sides ' symmetry, the outer tube impacted the inner rod with an impact angle close to 0 °. However, proper impact speed and impact angle are requirements for good welding conditions [17, 18]. Although the impact speed of the outer tube located in the central field shaper is the largest, effective joining was not observed in zone II as the impact angle of the outer tube is approximately 0 °, as shown in Fig. 3, the residual metal in peeling morphology increased with increasing discharge voltage, whereas zone II has no noticeable change, still belonging to an invalid joining area, indicating that just increasing impact speed cannot ensure suitable welding. However, tube deformation was generated along the axial direction of Zone II owing to higher impact speed, forming a proper impact angle between the center and both sides. Although impact speed may be lower than that of the center, the impact angle is larger, the effective joining zones I and III on both sides were formed when two sides impacted the inner rod [5] (Figure 3). It is noteworthy that both the deformation and impact angle are large for the outer tube of zone III adjacent to the non-deformed zone, leading to the highest joining strength. It is seen that shear strength gradually increased with increasing discharge voltage from the distribution trend of overall shear strength, which shows agreement with a study of MPW of Al-steel by Meng et al. [19]. They also observed that input energy and impact speed increased with increasing discharge voltage, resulting in more plastic deformation and improved shear strength.

3.1.2 Effect of the radial gap on joint quality

The shear strength and peeling morphology at different radial gaps are shown in Fig. 4. All the joints are divided into three areas, zone I (left), II (center), III (right), the shear strength of zone I gradually increased with increasing radial gap and variation of the content of residual metal and shear strength is consistent for zone I. Strength distribution in zone III shows that areas with shear strength above 30MPa increased greatly, and the effective joining area expanded at a radial gap greater than or equal to 1.75mm, deformation space of outer tube became large and impact angle formed between the outer tube and inner rod also increased, as shown in Fig. 5, which is more conducive to the formation of effective joining. However, Fig. 3(a) and Fig. 4(a) show that radial gap has a more significant effect on shear strength of zone I and zone III compared with discharge voltage, owing to the change of impact speed of outer tube by changing discharge voltages, while both of impact speed and impact angle changed significantly with the variation of the radial gap [7], thus shear strength changed distinctly.

3.1.3 Effect of overlapping length on joint quality

The shear strength and peel morphology of the joints as a function of overlapping lengths is shown in Fig. 6, where shear strength distribution at an overlapping length of 10 mm is U-shaped and the center part is an invalid joining area with a length of approximately 5 mm. Both two sides are effective joining areas with residual metal on the inner rod surface. As overlapping length is reduced to 8 mm, the joint can still be divided into three areas according to the distribution of joining strength. Wherein the length of the invalid joining area was reduced significantly. Because the initial impact point is closer to the free end of the outer tube at an overlapping length of 8 mm with the restraint of the free end is significantly reduced, indirectly changing the impact angle, meeting the demands for welding. At an overlapping length of 6 mm, joining strength is higher than 40MPa except for the left endpoint. A large amount of residual metal is observed in the inner rod, indicating an effective joining zone. However, the shear strength of the left endpoint is just 10MPa due to severe deformation of the outer tube, where the first shear sample was located, which is insufficient to reflect the real joining strength. At an overlapping length of 4mm, the whole joint belongs to effective joining, but the effective joining area is small. Therefore, the influence of overlapping length on shear strength is significant.

In conclusion, the invalid joining area gradually decreased with decreasing overlapping length. The whole joint belongs to effective joining at an overlapping length of less than or equal to 6 mm. However, most areas of the joints are invalid at an overlapping length of 9 mm and only a tiny amount of residual metal was observed in the inner rod at the non-free end. Li et al. [20] reported that all positions of the outer tube impacted the inner rod at the same time when the ratio of overlapping length and working area length reached about 0.92. However, the impact angle cannot satisfy the requirement of MPW, leading to a large area of invalid joining at an overlapping length of 9 mm.

3.1.4 Discussion on optimizing welding process window

According to the peel morphology (Fig. 7(a)), the joints can be divided into three types: failed weld, partial weld, and good weld. The failed weld with a small amount of residual metal on the inner rod surface. For the partial weld, the ratio of titanium rod length with residual metal to connection length is less than 30%. Moreover, the ratio is higher than 30% for the good weld. The process window determined according to the peel morphology is shown in Fig. 7(b).

The shear strength of the partial welds and good welds is shown in Fig. 8. Three samples were tested and the average highest shear strength was taken as the shear strength, wherein the highest shear strength was obtained with good welding stability at an overlapping length of 10 mm, discharge voltage of 6.5 kV and radial gap of 2 mm, respectively. Furthermore, Fig. 9 shows that the effective joining ratio η is close to 100% at an overlapping length of 6 mm with the highest effective joining length, indicating that the ideal overlapping length is 6 mm with a maximum shear strength of 58MPa, which is lower than that at an overlapping length of 10 mm.

3.2 Discussion on impact mode of the outer Al tube

3.2.1 Microstructure of joint surface at different overlapping lengths

Figure 10 shows microstructure along the longitudinal section at overlapping lengths of 10 mm, 9 mm, 6 mm, and 4 mm, respectively. The distribution of shear strength changed with variation of overlapping length by comparing mechanical properties and peel morphology at different overlapping lengths, indicating that the joining process changed in the process of MPWed Al-Ti.

At the overlapping length of 10 mm, the joint interface closed to the free end is shown in Fig. 10(a1). It has been tightly bonded with a uniformly distributed transition layer, showing an effective joining area. The shear strength is 50MPa, and the effective joining length of about 2-3mm, as observed in Fig. 6(a). Fig. 10 (a2) shows that the transition layer was not observed between BM of Al and Ti but with a crack gap, indicating an invalid joining at an overlapping length of 5mm. Fig. 10(a3) shows the microstructure of joint surface near the end of BM, indicating an effective joining with a shear strength of 65MPa, which is higher than that of the wavy surface with a transition layer, and effective joining area has a length of about 2-3mm with waves being observed. Yu et al. [21] pointed out that wave interface was caused by Helmholtz instability, and starting position of waves is regarded as an efficient impact starting point. As seen in Fig. 10 (b1), as the overlapping length decreased to 9 mm, there is a noticeable gap between Al and Ti from the free end to end of BM, because the outer tube impacted the inner rod at an angle parallel to the inner rod, which could not form an effective joining. However, the BM's end was constrained with an effective impact angle, resulting in a small area of tight joining (Fig. 10(b2). Fig. 10 (c) shows microstructure along the longitudinal section at an overlapping length of 6 mm, where Al and Ti were closely joined. Microstructure distribution is relatively regular in the whole joining range. The joint surface is divided into two types. The one is the joint surface with a discontinuous transition layer and a shear strength of 45MPa (Fig. 10 (c1)), which is similar to that of the joint with a transition layer of large thickness at an overlapping length of 10mm. And the other one is the wavy surface without transition layer (Fig. 10 (c2)) with a shear strength of 63Mpa.

The outer aluminum alloy tube has undergone severe deformation at the left side of point D, mainly caused by material flow when the outer tube impacted the inner rod at a higher impact speed. At the right side of point D, there are regular waves on the joint surface with its amplitude increasing gradually from point D to the right, thus point D is the initial point of the wave, namely, the initial point of impact. When overlapping length was reduced to 4mm, a thin transition layer was observed at point D1 with a shear strength of 48MPa, similar to the thick transition layer interface (Fig. 10(a2)). Therefore, the thickness of the transition layer has little influence on shear strength and there is a wavy feature with a small wavelength in the D2 zone with a maximum joining strength of 55MPa.

In conclusion, the strength of interface without a transition layer is greater than that with a transition layer in MPW joint of Al-Ti alloy, and the IMC Al_3Ti was found in the transition layer in session 3.3, reducing mechanical properties. However, noticeable waves were observed in the effective joining area according to microstructure (Fig. 10) and joining strength (Fig. 6). Meanwhile, the boundary point between wave and

invalid joining area is deemed as the initial point of the wave, namely, the starting point of efficient welding. Therefore, at an overlapping length of 10 mm, the central outer tube of the overlapping part first impacted the inner rod, then the impact extended gradually from center to both sides and the effective joining began at points A and B. At an overlapping length of 9mm reaching the equilibrium length, effective joining is hard to achieve without adequate impact angle until the point reached D. As the overlapping length was reduced to 6 mm and 4 mm, the impact position started from the free end, thus useful impact and effective joining started from point D to the end of joint.

3.2.2 Impact modes of the outer tube

The MPWed Al-Ti joints can be divided into three impact modes, bidirectional impact mode, overall impact mode and single orientation impact mode according to mechanical properties and cross-section characteristics of the joint surface at different welding parameters (Fig. 11). In bidirectional impact mode (Fig. 11(a1-a3)), the central overlapping area of the flyer impacted the inner rod firstly due to the maximum magnetic force in this area. And the impact angle is too small to achieve an effective joining area at this stage, which resulted in the invalid joining area at the central zone. As the impact progresses, the impact point shifts along the Ti bar surface horizontally on two opposite sides from the center. The impact angle is suitable for the welding conditions, forming the effective joining area at both ends as shown in Fig. 11(a3). In welded joints produced by overall impact mode at an overlapping length of 9 mm, the flyer impacted the rod at an angle nearly parallel to the inner rod (Fig. 11(b2)). It is hard to form an effective joining owing to the minor impact angle, only a tiny area of effective joining formed at the right side of the magnetic field zone (Fig. 11(b3)). In single-orientation impact mode, the initial impact point is close to the free end of the outer tube as shown in Fig. 11(c2). And then, the impact extended from the free end to the non-free end, and an effective joining formed in the whole overlapping area (Fig. 11(c3)) due to proper impact angle and impact speed.

3.3 The joining mechanism of the interface

3.3.1 Formation mechanism of different interfaces

As seen in Fig. 12, the welded joint is divided into four interfaces of transition layer: continuous transition zone, transition zone with cracks, intermittent transition zone and non-transition zone. During the MPW process, the flyer impacting the target caused severe shearing of the interface, initiated jetting phenomenon, and generated strong confined heating, which melts the metals at the interface, finally forming IMCs layers [22]. And the continuous transition zone was formed under sufficient impact energy. The intermittent transition zone occurred with decreasing impact energy. However, the non-transition zone was formed when impact energy was insufficient to melt the BM. During the cooling process, there is a noticeable radial temperature gradient owing to the high heat dissipation rate of the Al tube and the low heat dissipation rate of the Ti rod, resulting in higher radial stress and the formation of transition zone with cracks, as shown in Fig. 12(b). Many particles with different brightness were observed in the transition layer with a maximum thickness of 80μm in the continuous transition zone (Fig. 12(a)), owing to damage of the joint surface. Fig. 12(c) shows that BM on both sides fluctuated greatly in the

intermittent transition zone. The transition layer on the joint surface was primarily observed in the valley of the Ti side. The corrugated joining surface in the non-transition zone in Fig. 12(d) would indicate that deformation of the Al side is apparent owing to its FCC crystal structure with two essential characteristics of interface, waves and IMCs, respectively. The bonding mechanism of wave interface is mechanical bonding and the presence of IMCs would indicate that the bonding mechanism is metallurgical bonding. Therefore, the bonding mechanism of MPWed Al-Ti is a composite bonding consisting of mechanical bonding and metallurgical bonding.

3.3.2 Effect of waves on mechanical properties of joints

As seen in Fig. 10, wavy features were observed in effective joining area, even in joint surface with transition layer, this meant that waves are the prerequisite for effective joining of Al-Ti MPW. Uhlmann et al. [23] studied the MPW process of Al alloy and found that waves are a prerequisite to ensure high-quality welding at different wave sizes. Fig. 13 shows the morphology of joint surface at different welding parameters and amplitudes of waves in Fig. 13(a) and Fig. 13(b) are 20μm and wavelengths in Fig. 13(a) and Fig. 13(b) are 200μm and 160μm with joining strength of 48MPa and 60MPa, respectively, indicating that joints with smaller wavelength have higher shear strength at the same wave amplitude. The wavelengths in Fig. 13(c) and Fig. 13(d) are 40μm, wave amplitude of interface in Fig. 13(c) and Fig. 13(d) are 4μm and 7μm with joint joining strength of 55MPa and 63Mpa, respectively. Therefore, the joints with higher wave amplitude have higher shear strength at the same wavelength. Raoelison et al. [24, 25] also found that higher wave amplitude has led to higher shear strength. Moreover, wave amplitude increased with increasing impact energy, which has enhanced the shear strength. To sum up, the formation of waves is a necessary condition for an effective joining.

3.3.3 Analysis of intermetallic compounds on the interface

Figure 14 shows the EDS results of the transition zone at an overlapping length of 8mm, where points 1 and 2 are light grey and dark grey areas in the transition layer, respectively. From the scanning results of point 1, the atomic mass of Al and Ti are 64.88% and 35.12%, respectively, which is the Al_3Ti phase. Therefore, Al_3Ti was also formed during the MPW process of Al and Ti, as proposed by Sun et al. [26] and Miao et al. [27]. The element content of point 2 shows that the atomic mass of Al and Ti is 95.89% and 4.11%, respectively. Therefore, Al3Ti and some of Al BM were observed in the transition layer because an intense collision occurred between the outer tube and inner rod during the MPW process with sufficient welding energy. At the same time, 1060 Al with relatively low mechanical properties was broken. Some aluminum fragments were embedded in the joint surface owing to short welding time and rapid cooling rate. In addition, aluminum fragments in the joint surface have not been completely melted, thus it retained in the transition layer.

Figure 15 shows hardness results of different joint surfaces with indentations, wherein hardness distribution of joint surface and the dotted line is at the initial edge of Ti rod. The average hardness of Ti BM and Al BM is 200 HV and 50 HV, respectively, in the interface of the non-transition layer and hardness changed distinctly at the joint surface since the hardness of Al and Ti is 17HV and 125HV, respectively.

This meant a significant difference between the hardness of the two sides of the BM and joint surface. It is noteworthy that the hardness of both sides of the joint surface is higher than that of the BM and hardness increased with decreasing distance from the BM. The maximum hardness of the Al side at joint surface reached 75HV, owing to severe plastic deformation generated at the interface, resulting in grain refinement and work hardening was also an influencing factor [28, 29]. As seen in Figure 15(d), the hardness of the transition layer at both sides is greater than that of the BM and hardness increased with decreasing distance to the interface. It is noteworthy that the hardness of the transition layer is in the range of the Al and Ti BM owing to Al_3Ti in the transition layer, which is a brittle compound with poor plasticity and poor toughness at room temperature [30]. Therefore, although IMCs were produced in MPW of Al-Ti owing to high impact energy, the IMCs are not necessary to ensure effective joining of Al-Ti by MPW.

3.3.3 Joining mechanism of Al-Ti MPW joint

According to previous reports [17, 18] and the results of this paper, the reliable impact speed and impact angle are the critical factors for Al-Ti MPW. Proper discharge voltage, radial gap and overlapping length are required for the MPW process of dissimilar Al and Ti. The wave interface and intermediate transition layer composed of IMCs are the two major characteristics of MPWed Al-Ti. All the effective joining joints have regular waves, the formation of which is a necessary condition for effective joining. The characteristic of the IMC transition layer is relatively complex. Although most efficient joining areas have an IMC transition layer, some areas without an IMC transition layer also achieved effective joining.

Moreover, a small amount of IMCs cracked lead to failure of the Al-Ti joint. The formation of IMCs would indicate that the outer tube's impact speed and impact angle are proper. However, IMC is unnecessary to achieve effective joining because only the joints with waves achieved effective joining in overall impact mode. At the same time, IMCs were formed in the joint interface at proper impact speed and impact angle due to the hard and brittle characteristics of IMCs, contributing to cracking and joining failure.

To conclude, the wave interface is a necessary condition to achieve effective joining during the MPW process. The generation of wave interface owing to sufficient process parameters is also an essential factor in improving shear strength by mechanical interlock generated by the wavy interface. The IMCs proved effective in impacting the outer tube, but the IMCs are not the necessary condition to obtain a good joining due to their hard and brittle characteristics.

4 Conclusions

This paper investigates the influence of overlapping length on impacting modes and joining mechanism for MPW of dissimilar 1060 Aluminum and TA1 titanium alloys and the process window is summarized. The conclusions are shown as follows.

1. Three impact modes were identified for MPW of Al-Ti: a. bidirectional impact mode when the overlapping length is equal to the working area length of field shaper; b. the overall impact mode when

the overlapping length is close to 92% of the working area length; c. the single-orientation impact mode with highest effective joining ratio when the overlapping length is less than 60% of the working area length.

2. The interface of the MPWed Al-Ti joint has two characteristics: waves and IMCs. Wave is a necessary condition to achieve effective joining. The IMC is not a necessary condition neither to achieve effective joining nor to improve the shear strength.

3. The shear strength is the highest at the overlapping length of 10 mm, discharge voltage of 6.5 kV, and radial gap of 2 mm. At an overlapping length of 6 mm, the effective joining ratio is the highest, which is the ideal overlapping length.

Declarations

Competing Interests and Funding

Conflicts of Interest: The authors declared that they have no conflicts of interest in this work.

Funding: This research was funded by the National Natural Science Foundation of China, grant number 51704013, 52075009.

References

1. Manladan SM, Yusof F, Ramesh S, Fadzil M, Luo Z, Ao S (2017) A review on resistance spot welding of aluminum alloys. Int J Adv Manuf Tech 90:605–634
2. Liu F, Fu L, Chen H (2018) High speed friction stir welding of ultra-thin AA6061-T6 sheets using different backing plates. J Manuf Process 33:219–227
3. Jin HX, Wei KX, Li JM et al (2015) Research progress of titanium alloys for aviation. Chin J Nonferrous Met 25(02):280–292
4. Kore SD, Date PP, Kulkarni SV (2008) Electromagnetic impact welding of aluminum to stainless steel sheets. J Mater Process Tech 208:486–493
5. Lu Z, Gong W, Chen S, Yuan T, Kan C, Jiang X (2019) Interfacial microstructure and local bonding strength of magnetic pulse welding joint between commercially pure aluminum 1060 and AISI 304 stainless steel. J Manuf Process 46:59–66
6. Manogaran AP, Manoharan P, Priem D, Marya S, Racineux G (2014) Magnetic pulse spot welding of bimetals. J Mater Process Tech 214:1236–1244
7. Yu H, Xu Z, Fan Z, Zhao Z, Li C (2013) Mechanical property and microstructure of aluminum alloy-steel tubes joint by magnetic pulse welding. Mat Sci Eng A-Struct 561:259–265
8. Yu HP, Xu ZD, Jiang HW, Zhao ZX, Li CF (2012) Magnetic pulse joining of aluminum alloy–carbon steel tubes. T Nonferr Metal Soc 22:s548–s552

9. Geng H, Xia Z, Xu Z, Li G, Cui J (2018) Microstructures and mechanical properties of the welded AA5182/HC340LA joint by magnetic pulse welding.Mater Charact138
10. Geng H, Mao J, Zhang X, Li G, Cui J (2019) Formation mechanism of transition zone and amorphous structure in magnetic pulse welded Al-Fe joint. Mater Lett 245:151–154
11. Peng N, Hou Z, Wang Z, Duan M (2018) Experimental study on electromagnetic pulse welding of aluminum and titanium plate. Machinery Design & Manufacture 07:90–92
12. Cui J, Ye L, Zhu C, Geng H, Li G (2020) Mechanical and Microstructure Investigations on Magnetic Pulse Welded Dissimilar AA3003-TC4 Joints. J Mater Eng Perform 29:712–722
13. Yong KB (2015) Review of magnetic pulse welding. J Weld Join 33(1):7–13
14. Wang S, Zhou B, Zhang X, Sun T, Li G, Cui J (2020) Mechanical properties and interfacial microstructures of magnetic pulse welding joints with aluminum to zinc-coated steel. Mat Sci Eng A-Struct 788:139425
15. Marya M, Marya S, Priem D (2005) On The Characteristics of Electromagnetic Welds Between Aluminium and other Metals and Alloys. Weld World 49:74–84
16. Fan Z (2012) Investigation on magnetic pulse cladding of 3A21 aluminum–steel 20 tube. Dissertation, Harbin Institute of Technology
17. Lee KJ, Kumai S, Arai T, Aizawa T (2007) Interfacial microstructure and strength of steel/aluminum alloy lap joint fabricated by magnetic pressure seam welding. Mat Sci Eng A-Struct 471:95–101
18. Wu X, Shang J (2014) An Investigation of Magnetic Pulse Welding of Al/Cu and Interface Characterization. J Manuf Sci E-T Asme 136
19. Meng Z, Peng Y, Yu L, Huang S, Lin H (2015) Effects of process parameters on the mechanical properties and microstructure of Al-steel joint by magnetic pulse welding. Matec Web of Conferences 21:11005
20. Li Z, Li CF, Zhao ZH (2008) Transient distribution of magnetic pressure in electromagnetic tube bulging. Mater Sci Tech-Lond 16:301–305
21. Yang Y, Chen S, Yu X, Lu Z (2012) Study on Wave Formation Mechanism in Magnetic Pulse Welding Rare Metal Mat Eng. S2:54–58
22. Li J, Sapanathan T, Nirina RR, Hou Y, Rachik M (2021) On the complete interface development of Al/Cu magnetic pulse welding via experimental characterizations and multiphysics numerical simulations. J Mater Process Tech 296:117185
23. Uhlmann E, Ziefle A (2010) Modelling Pulse Magnetic Welding Processes. fakultäten
24. Raoelison RN, Buiron N, Rachik M, Haye D, Franz G (2012) Efficient welding conditions in magnetic pulse welding process. J Manuf Process 14:372–377
25. Raoelison RN, Buiron N, Rachik M, Haye D, Franz G, Habak M (2013) Study of the elaboration of a practical weldability window in magnetic pulse welding. J Mater Process Tech 213:1348–1354
26. Sun J, Cao R, Chen J (2015) Analysis of welding-brazing joints of Ti/Al dissimilar metals obtained by cold metal transfer method. Transactions of the China Welding Institution 36:51–54

27. Miao YG, Wang T, Zhou Y, Han D (2015) Characteristics and mechanical properties of bypass-current MIG welding-brazed dissimilar Al/Ti joints. Transactions of the China Welding Institution 36(01):47–50
28. Chen S, Daehn GS, Vivek A, Liu B, Lin S (2016) Interfacial microstructures and mechanical property of vaporizing foil actuator welding of aluminum alloy to steel. Mat Sci Eng A-Struct 659:12–21
29. Cui J, Li Y, Liu Q, Zhang X, Xu Z, Li G (2018) Joining of tubular carbon fiber-reinforced plastic/aluminum by magnetic pulse welding. J Mater Process Tech 264:273–282
30. Li T, Grignon F, Benson D, Vecchio K, Olevsky E, Jiang F, Rohatgi A, Schwarz R, Meyers M (2004) Modeling the elastic properties and damage evolution in Ti-Al 3Ti metal–intermetallic laminate (MIL) composites. Mater Sci Eng A-Struct 374:10–26

Figures

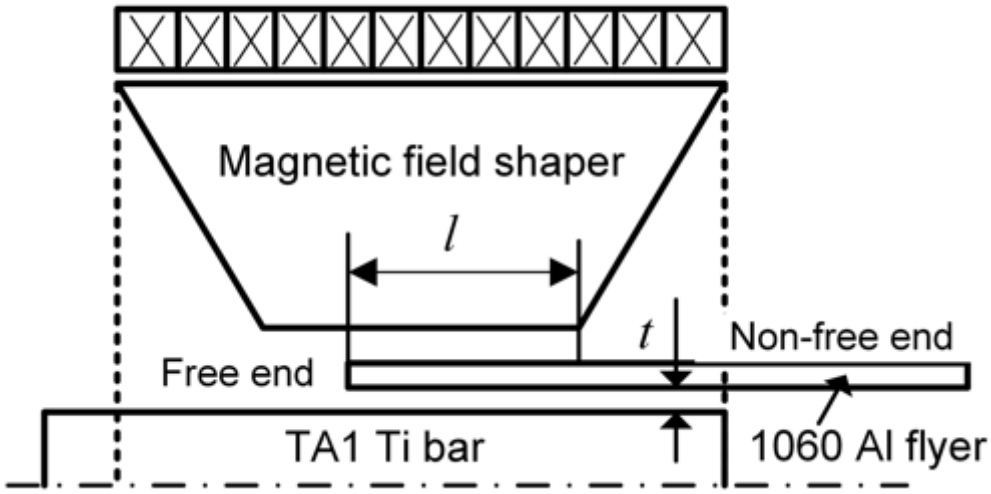

Figure 1

Schematic of the MPW process of Al flyer and Ti rod

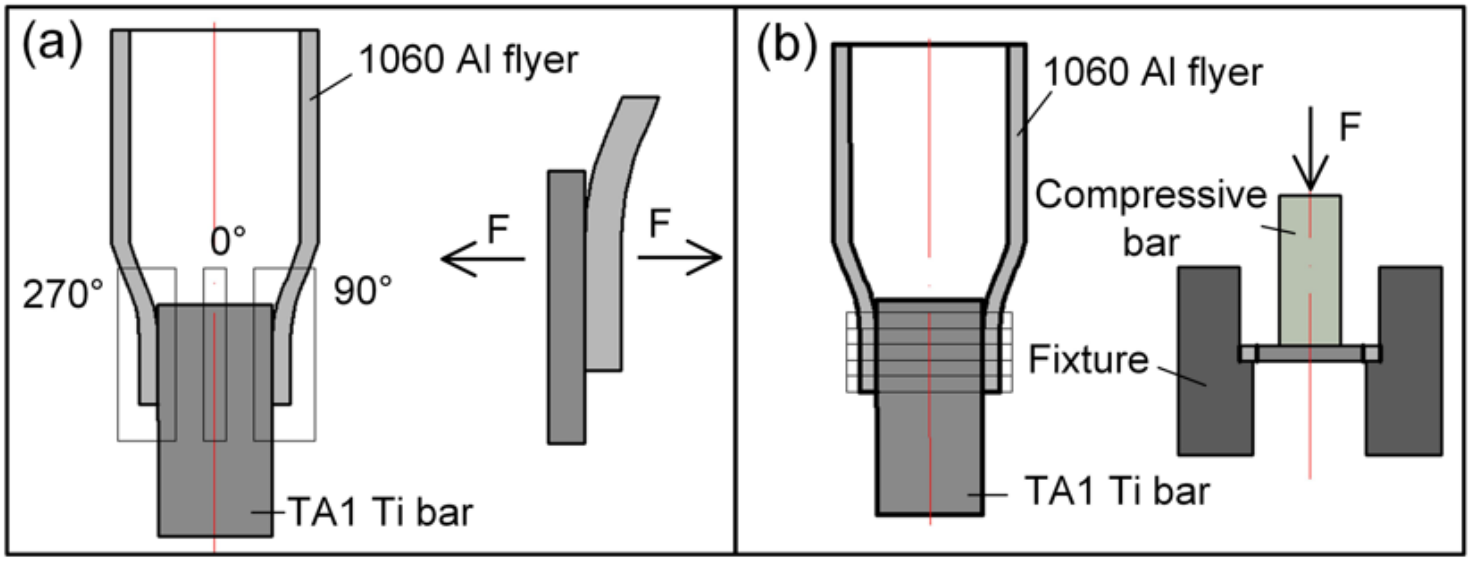

Figure 2

Diagrams of the peeling test and shear test

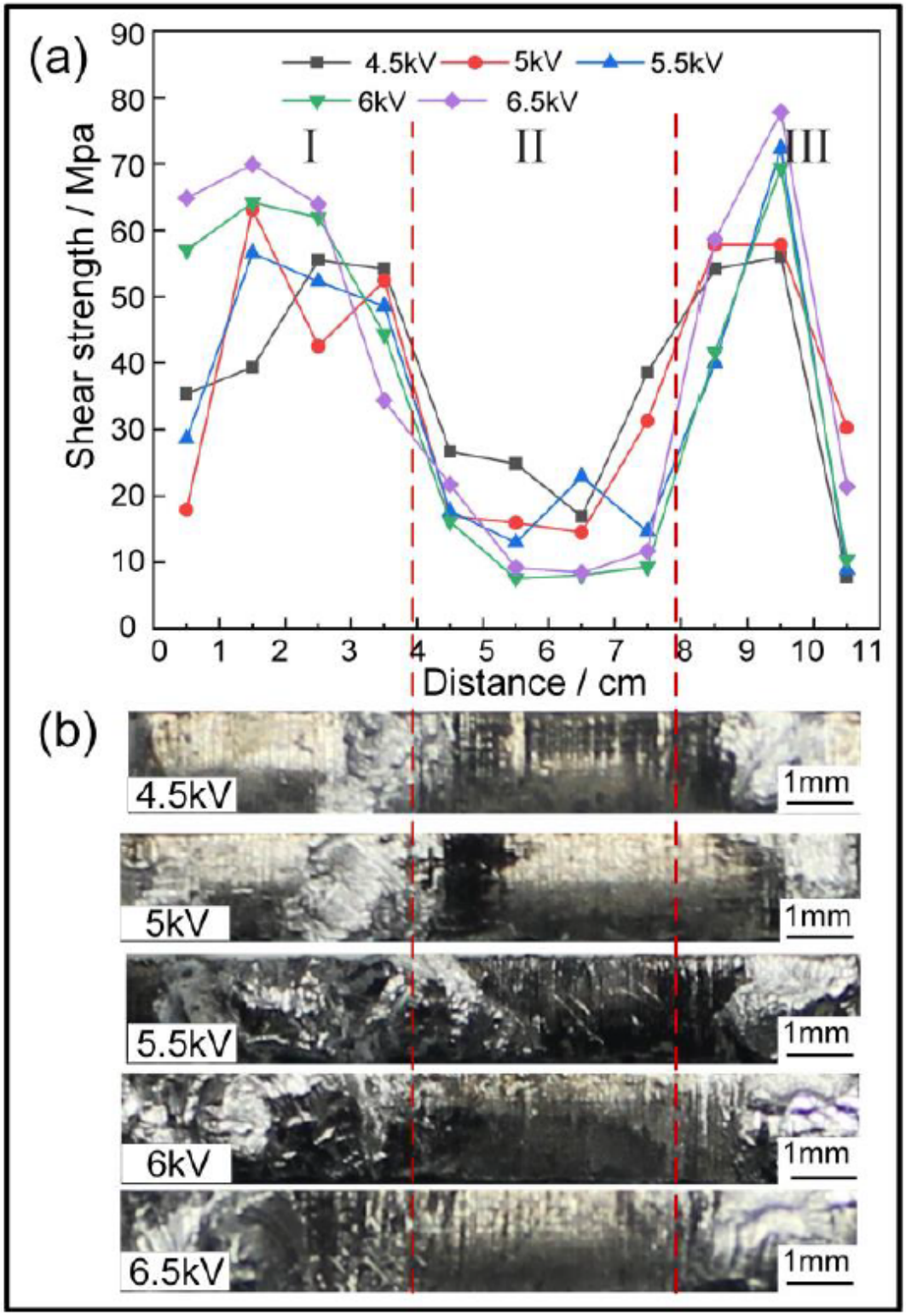

Figure 3

Distribution trend of joining strength and stripping morphology of the joints at different discharge voltages（t=1.75mm, l=10mm）

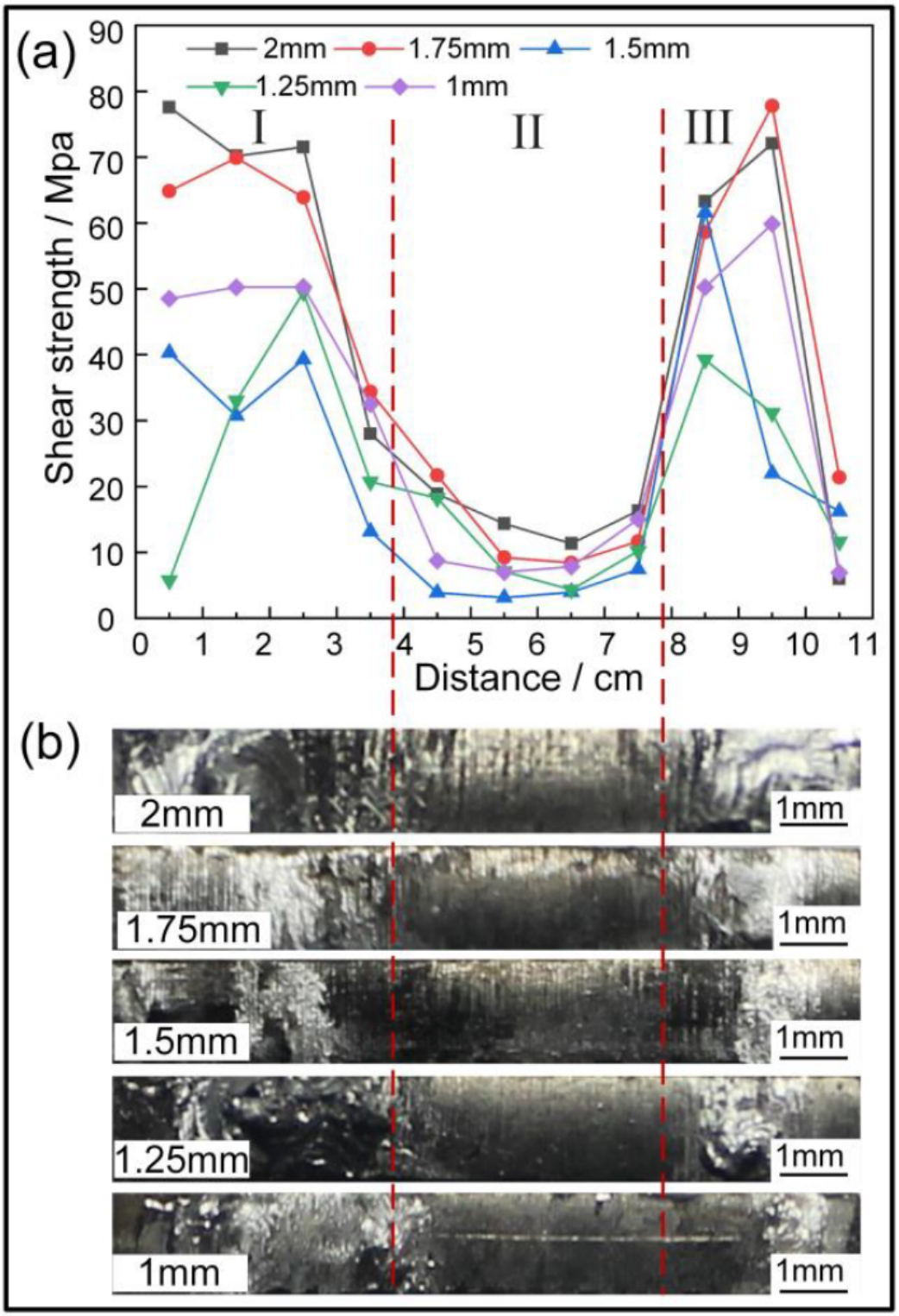

Figure 4

Joining strength distribution trend and stripping morphology of the joints at different radial gaps （V=6.5kV, l=10mm）

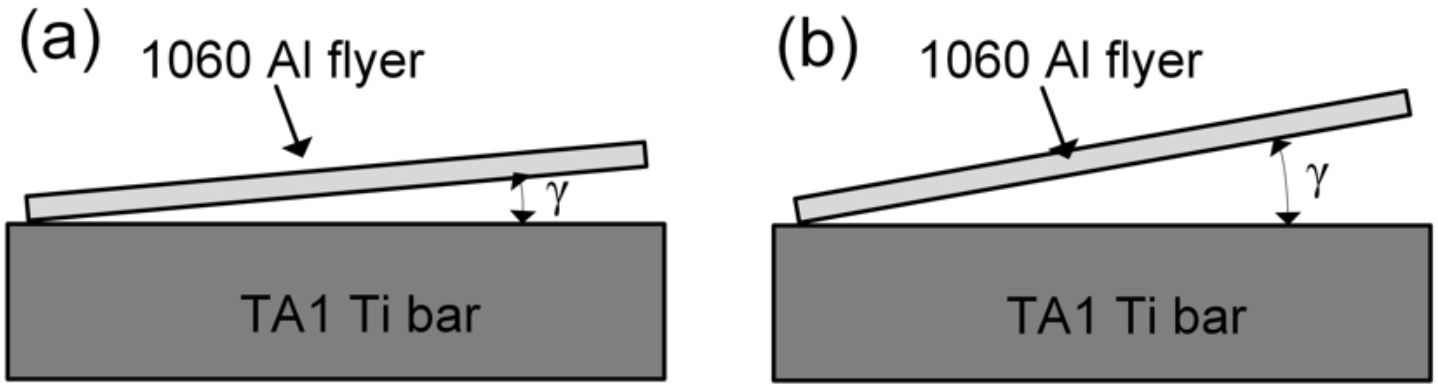

Figure 5

Schematic of the impact angle γ at different radial gaps: (a) small and (b) large radial gap

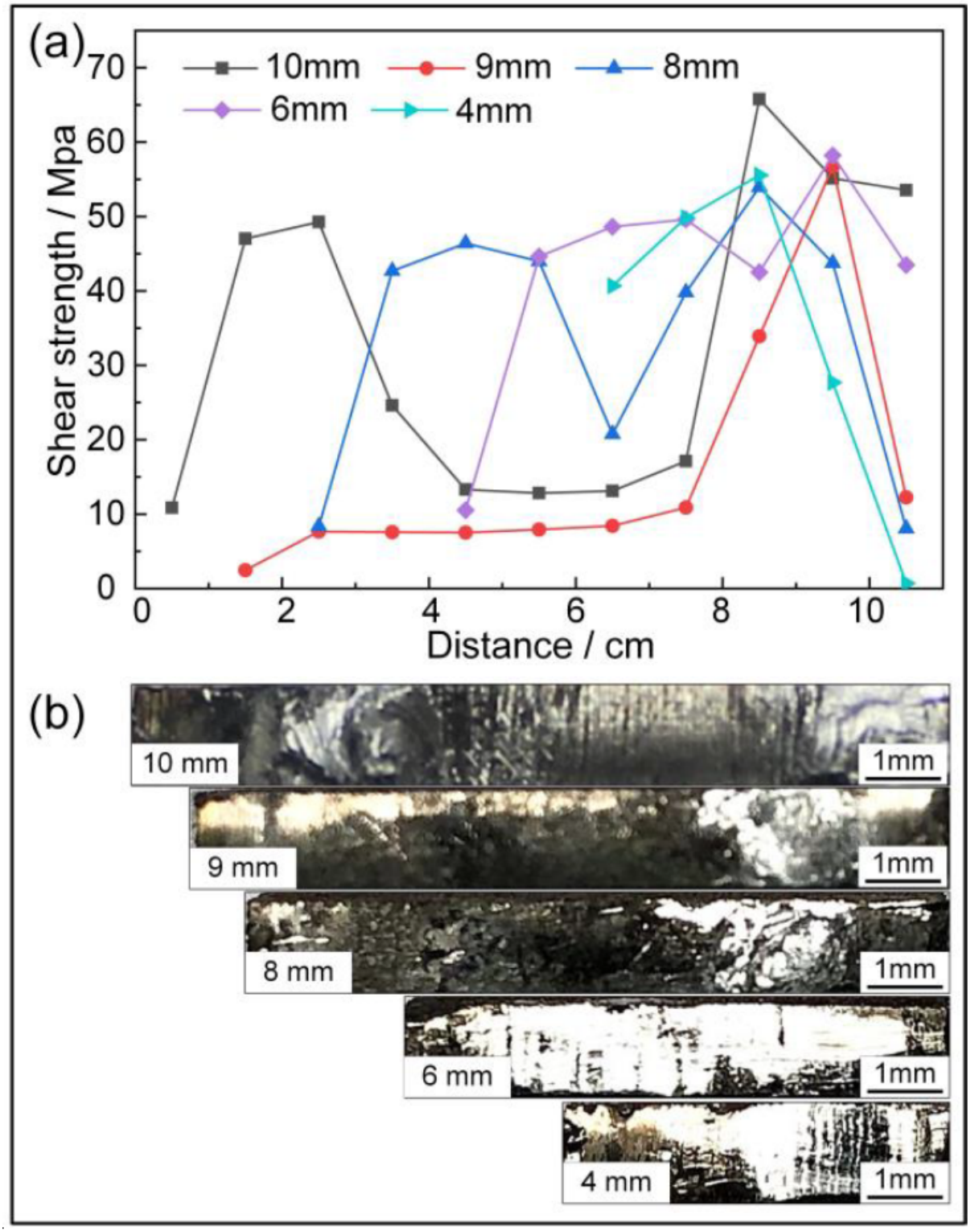

Figure 6

Joining strength distribution trend and morphology of the joints at different overlapping lengths (V=6.5kV, t=2mm)

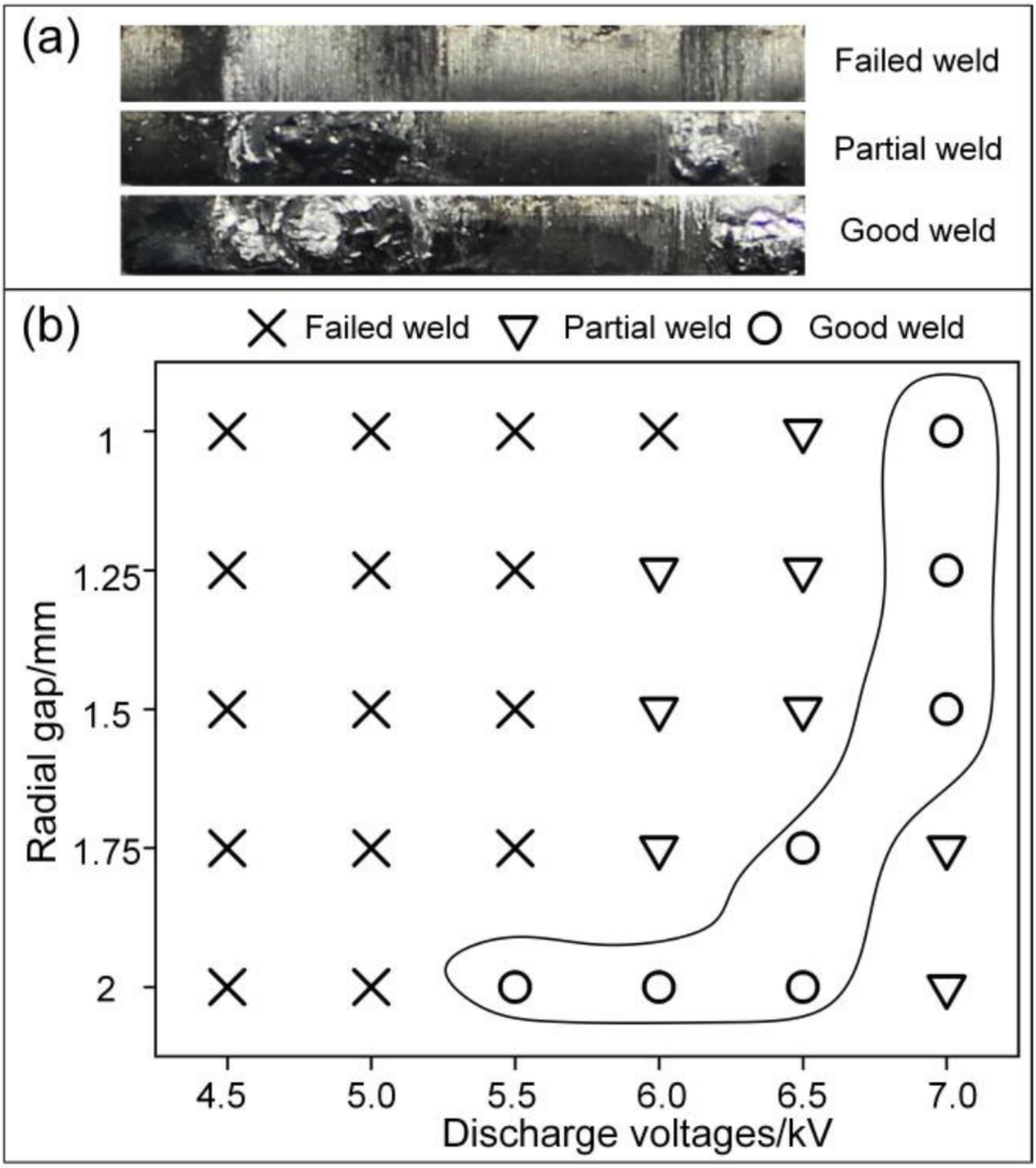

Figure 7

Evaluation standard for Peel morphology of welded joints and the welding process window

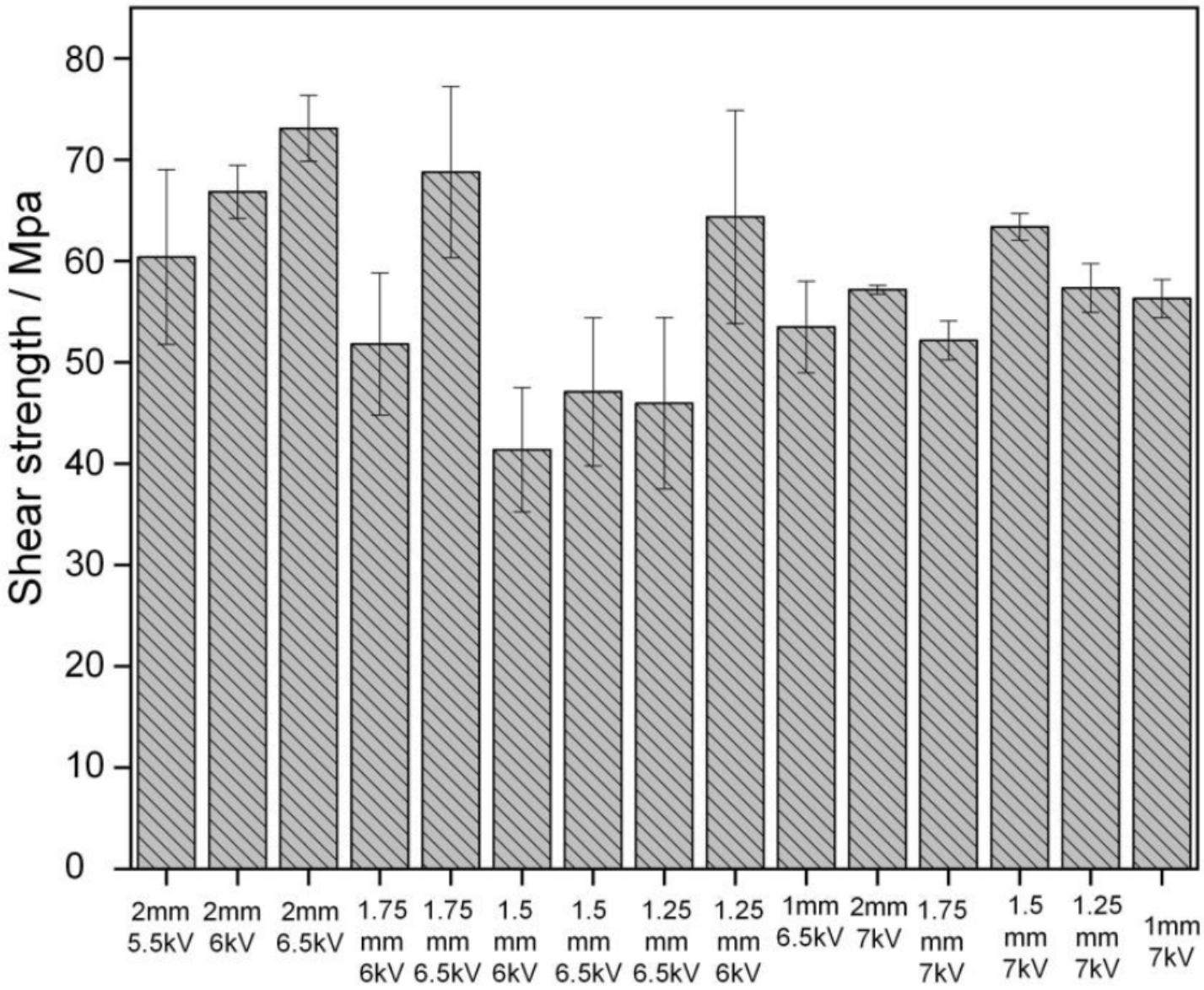

Figure 8

The shear strength at different welding process parameters (l=10mm)

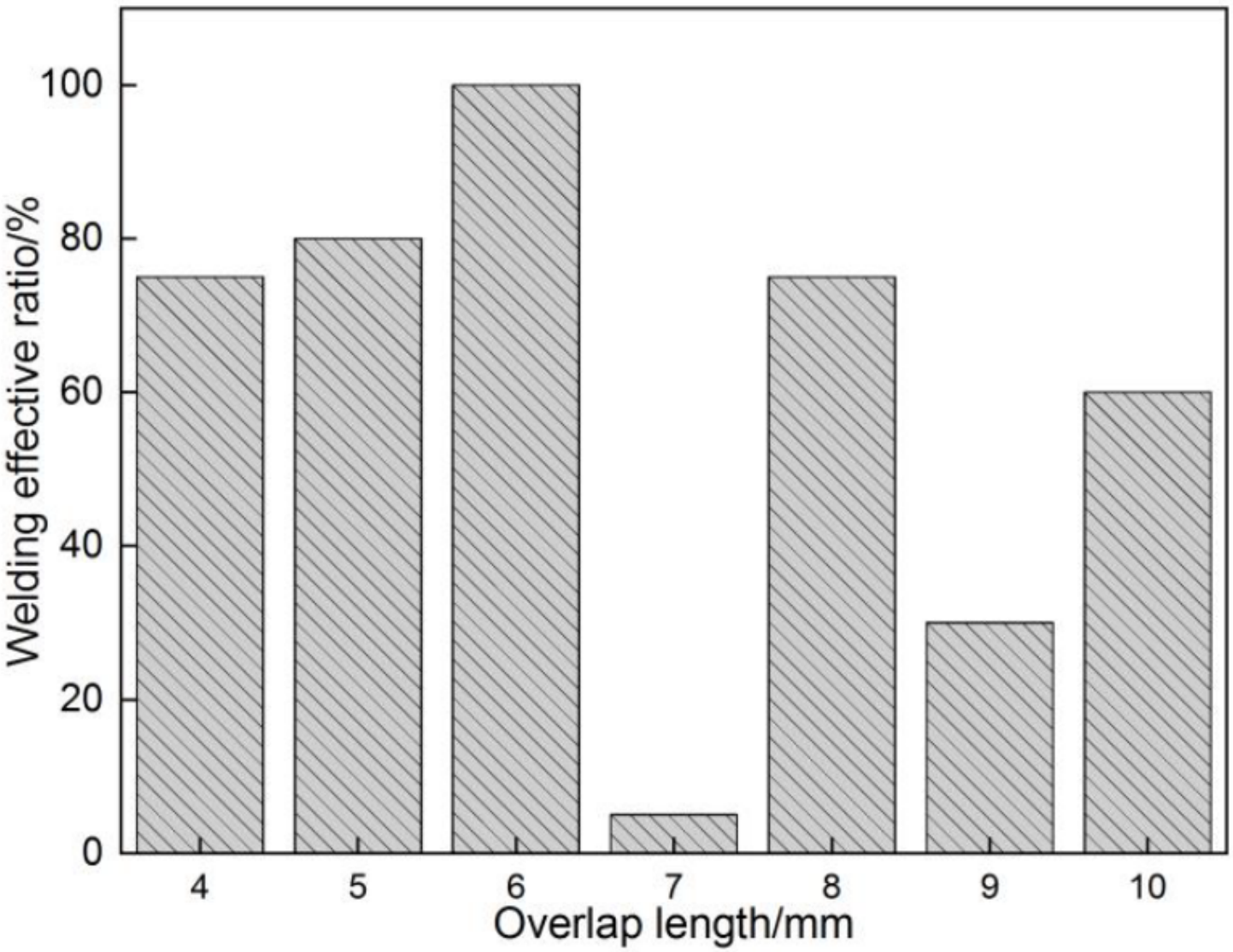

Figure 9

Effective joining length ratio at different overlapping lengths

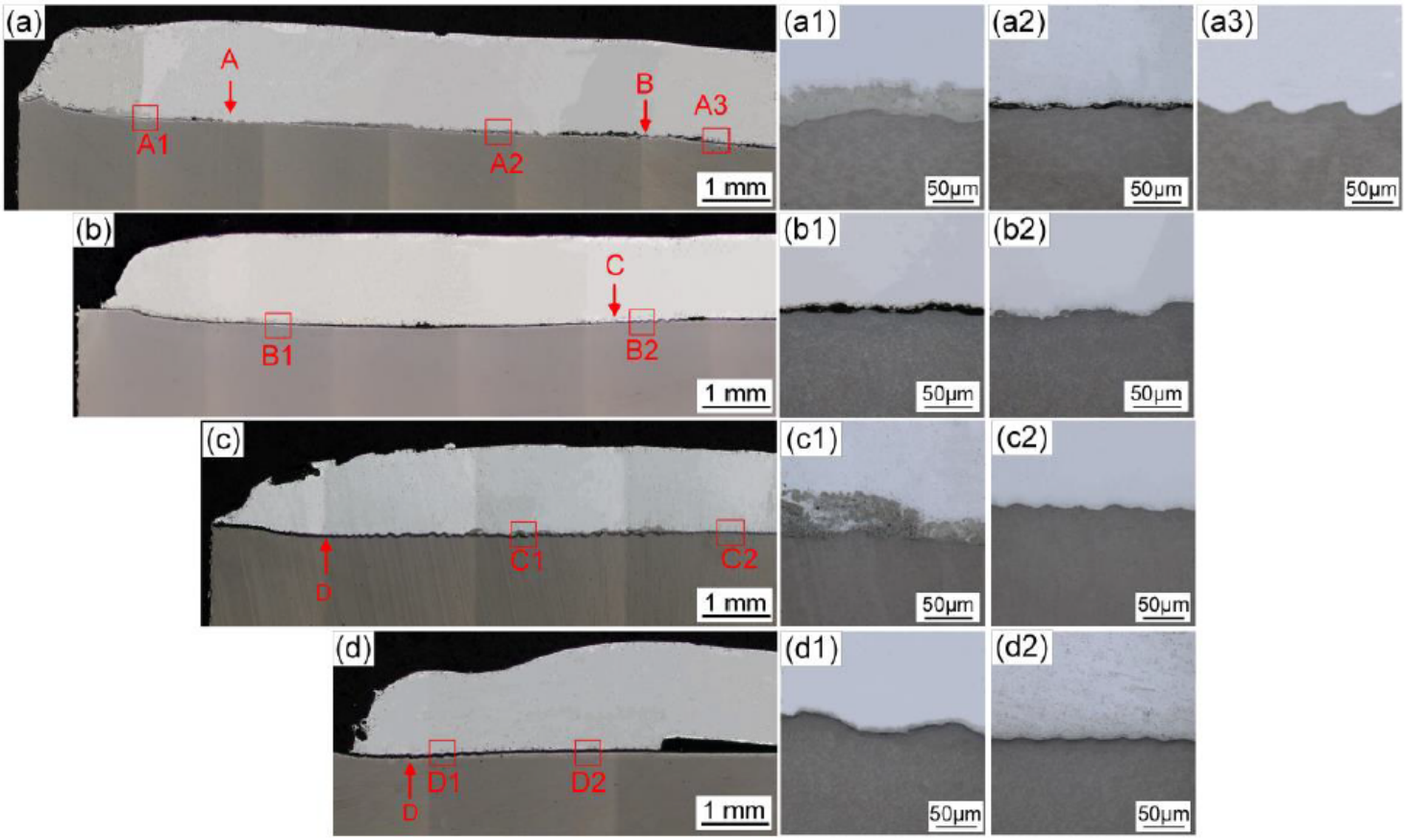

Figure 10

Stitched macrographs of the cross-section at an overlapping length of (a) 10 mm, (b) 9 mm, (c) 6mm, (d) 4mm; (a1)-(d1) are enlarged graphs of the points (A1)-(D1), respectively; (a2)-(d2) are enlarged graphs of the points (A2)-(D2), respectively; (a3) is enlarged graph of the point (A3)

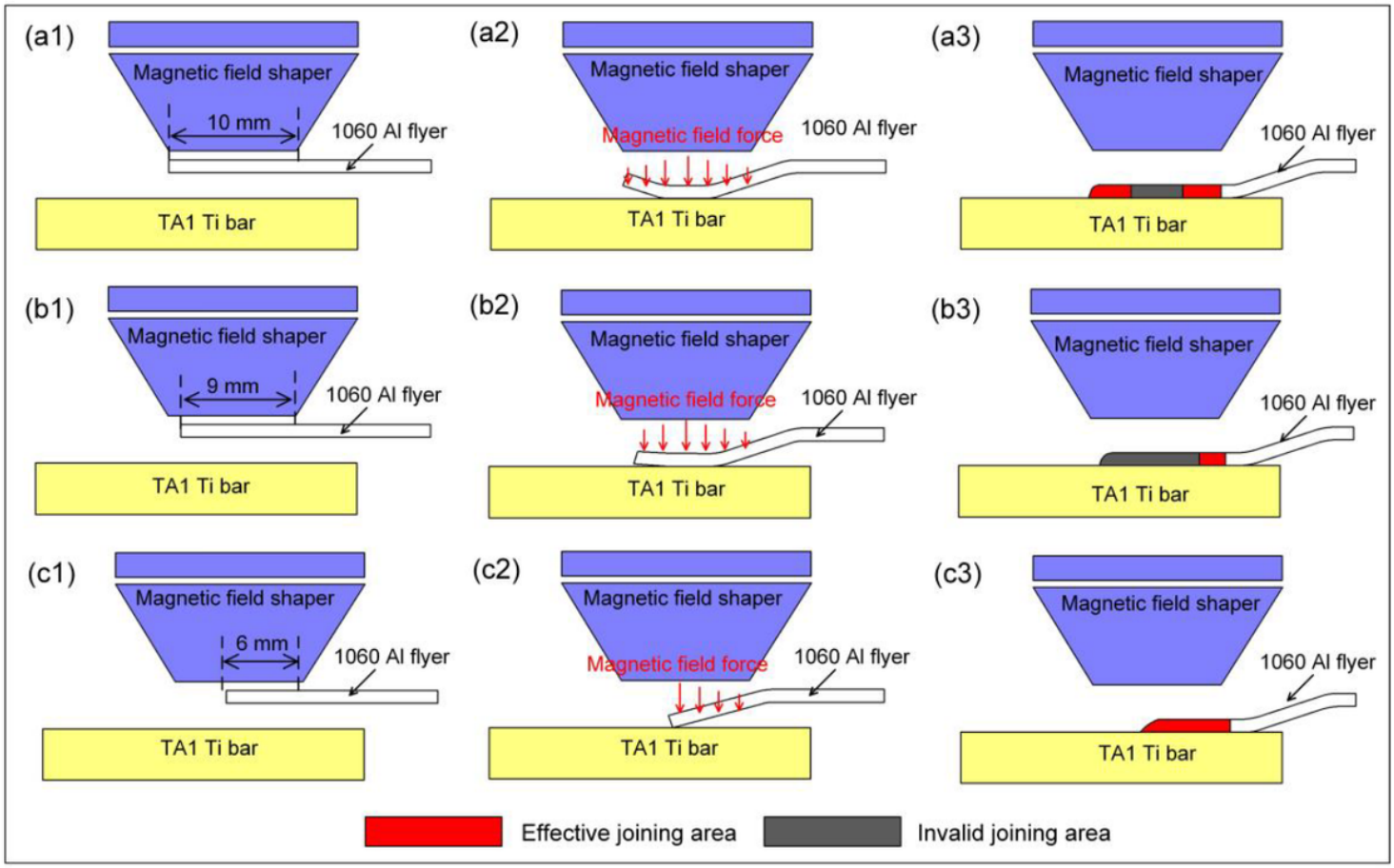

Figure 11

MPW process of Al and Ti: (a1-a3) bidirectional impact mode, (b1-b3) overall impact mode and (c1-c3) single-orientation impact mode

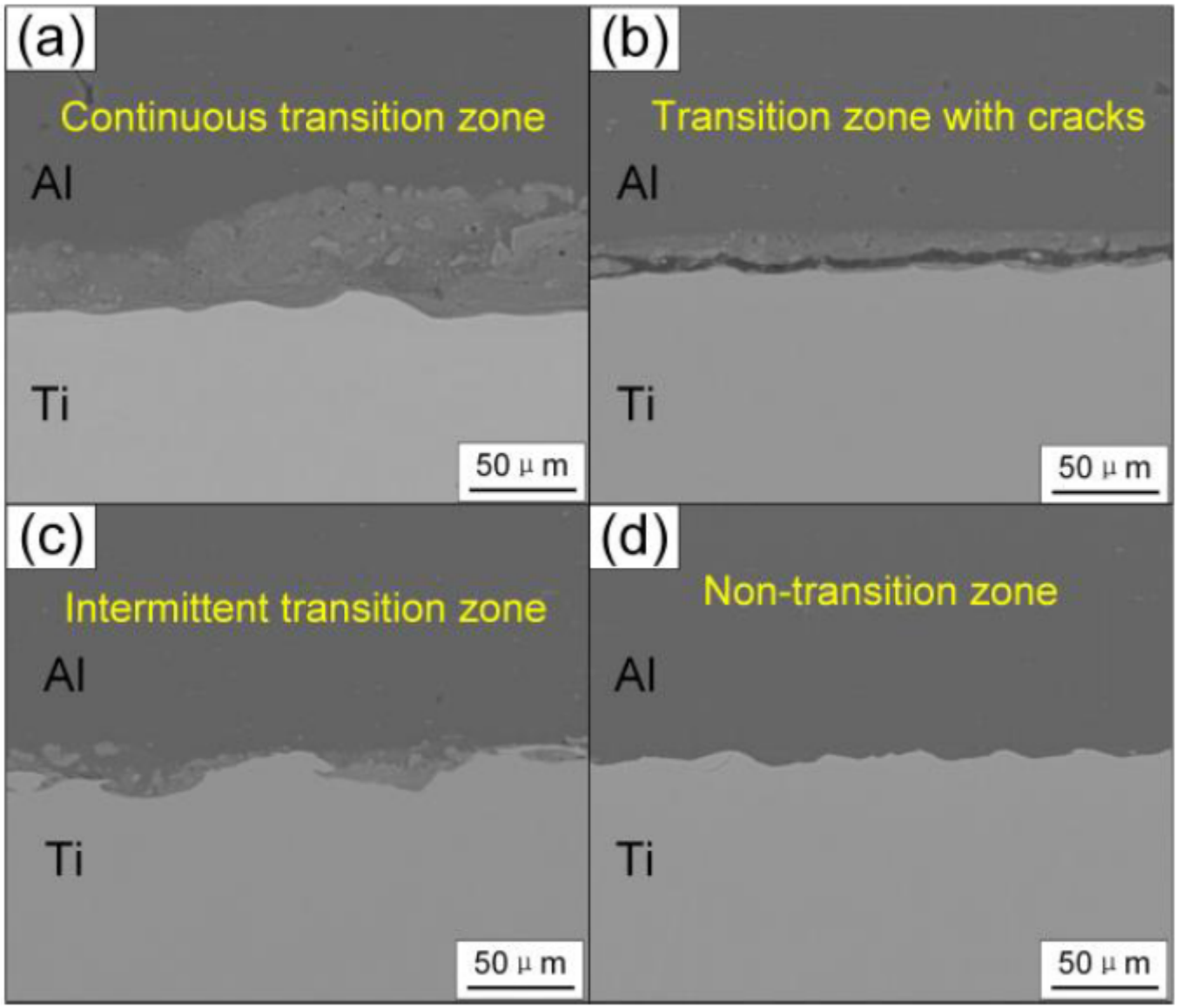

Figure 12

Morphology of joint interfaces: (a) continuous transition zone, (b) cracks in the transition zone, (c) intermittent transition zone, (d) non-transition zone

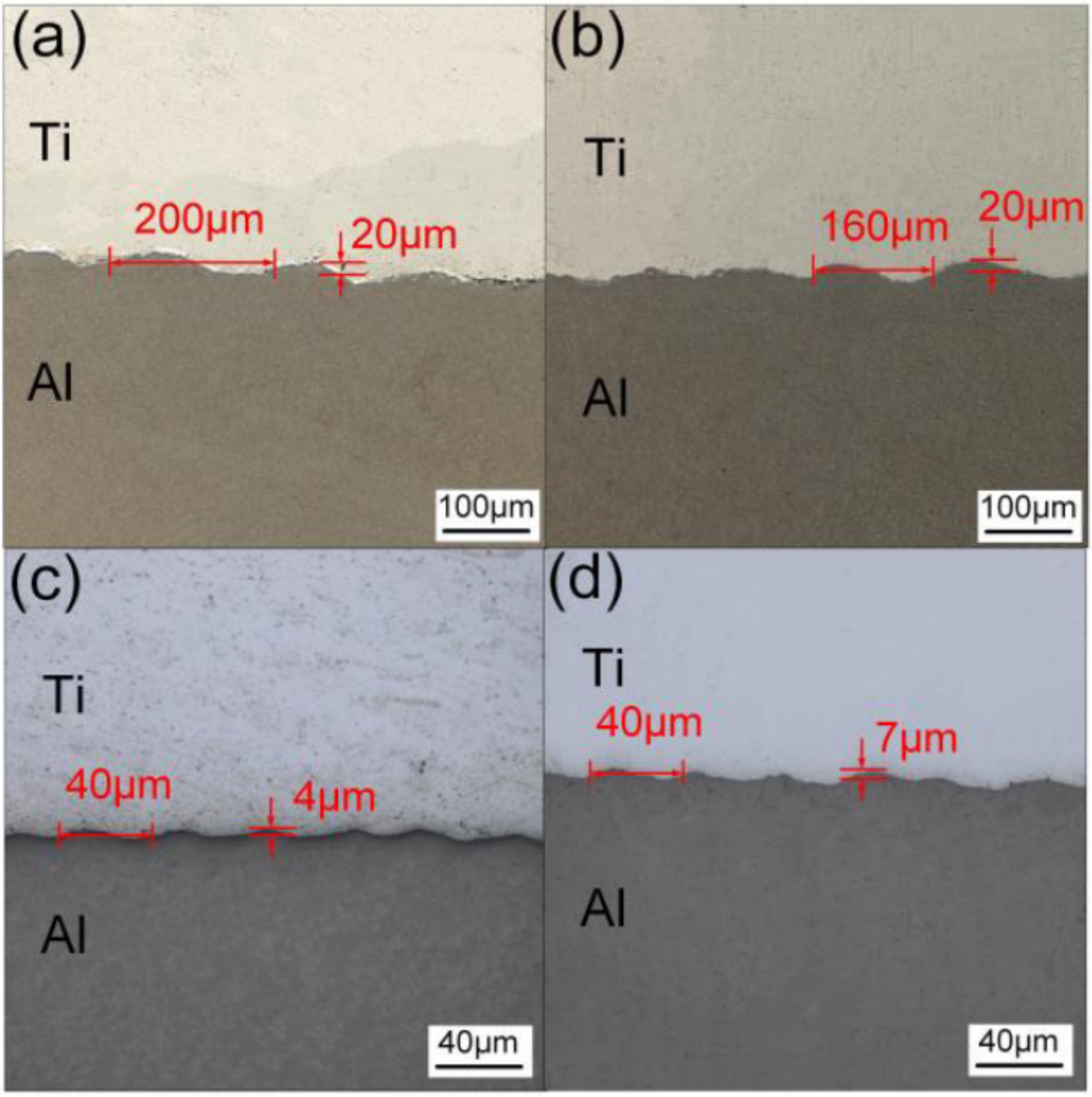

Figure 13

The wave interfaces at different wavelengths and amplitudes. (a), (c) are enlarged graphs of points D1 and D2 in Fig. 9(d), (b) is an enlarged graph of point B2 in Fig. 9(b), (d) is an enlarged graph of point C2 in Fig. 9(c)

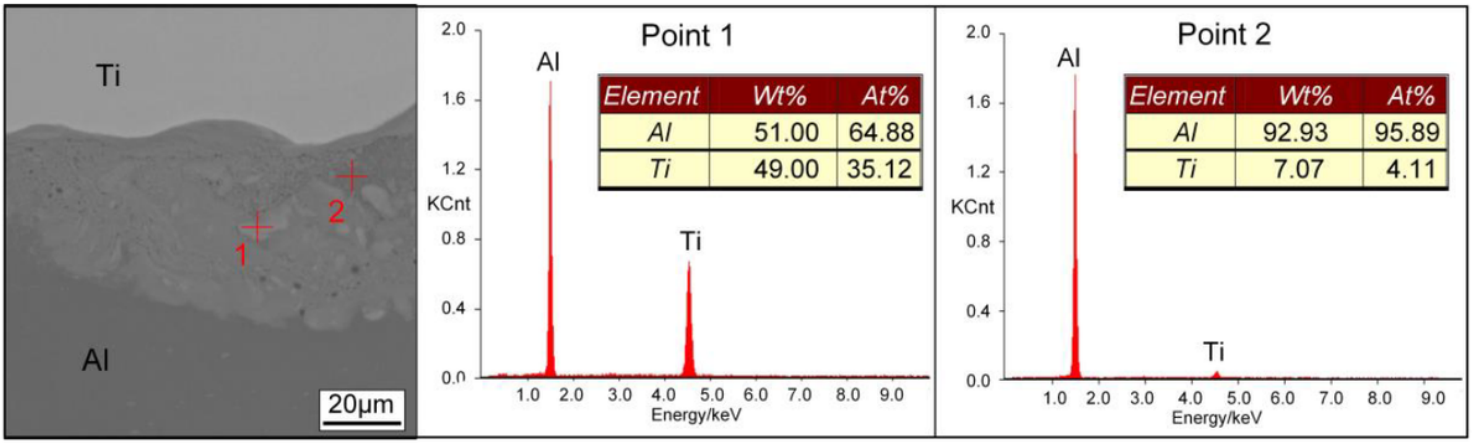

Figure 14

EDS result of the transition zone

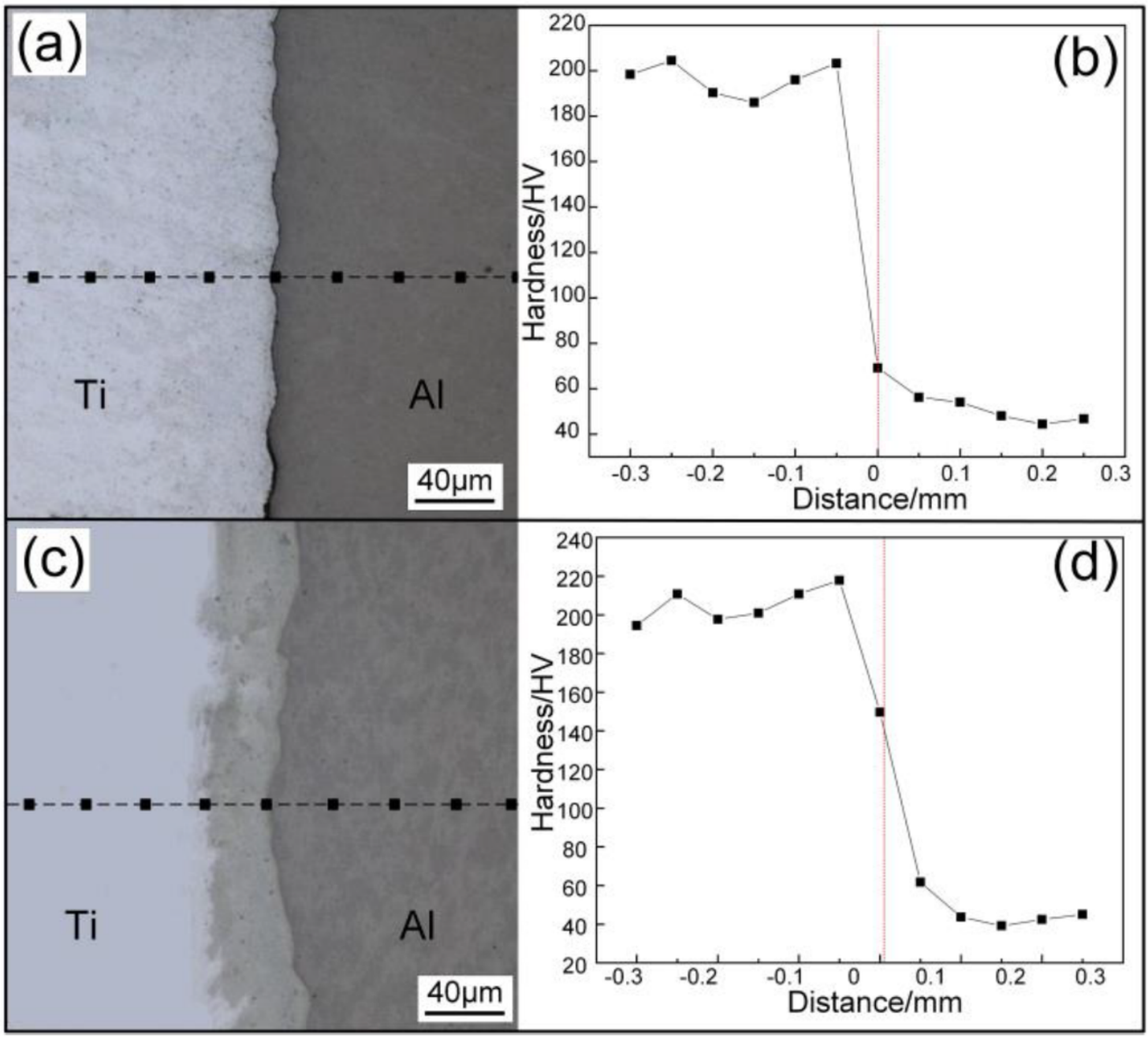

Figure 15

Hardness of the joints: (a) sampling locations and (b) hardness distribution of the non-transition zone; (c) sampling locations and (d) hardness distribution of the transition zone